

## FROM ULTRACOMPACT TO EXTENDED HII REGIONS: CLOUD GRAVITY AND STELLAR MOTION

Guillermo García-Segura<sup>1</sup> and José Franco<sup>2</sup>

### RESUMEN

Se estudia la evolución dinámica de regiones HII con y sin movimiento estelar en nubes moleculares densas y estructuradas. La gravedad de las nubes es simulada mediante una fuerza externa independiente del tiempo. Se consideran varios casos con diferentes velocidades estelares y distribuciones de densidad del gas. En los casos con movimiento, las estrellas se mueven desde el núcleo de la nube hasta el borde y viceversa. Cuando las estrellas se desplazan a regiones de baja densidad, ocurren transiciones desde ultracompactas a regiones HII extendidas, así como el comportamiento opuesto. La conclusión principal de nuestro estudio es que las regiones HII ultracompactas son entidades confinadas por presión mientras que permanezcan en los núcleos densos. El confinamiento en este estudio es producido por la presión térmica, por la presión dinámica, o por combinación de las mismas. La supervivencia como región ultracompacta sólo depende del tiempo de vida estelar y del tiempo de cruce del núcleo de la nube.

### ABSTRACT

The dynamical evolution of HII regions with and without stellar motion in dense, structured molecular clouds is studied. The cloud gravity is taken into account and is simulated by a time-independent, external force. Several cases, with different stellar velocities and gas density distribution are considered. When stellar motion is considered, stars are allowed to move from the central core to the edge of the cloud and vice versa. There are transitions from ultracompact to extended HII regions as the stars moves into lower density regions. However, the opposite behavior is also feasible when stars fall into the cloud core. The main conclusion of our study is that ultracompact HII regions are pressure-confined entities as long as they remain embedded within dense cores. The confinement in this study comes from either ram or thermal pressures, or a combination of both. Their survival as ultracompact regions only depends on the stellar life-time and on the crossing time of the cloud core.

*Key Words:* **HII REGIONS — ISM: BUBBLES**

### 1. INTRODUCTION

Ultracompact HII regions (UCHIIs) have been extensively studied in surveys by Wood & Churchwell (1989) and by Kurtz et al.(1994). Those surveys revealed that UCHIIs can be classified as: cometary (20%), shell (4%), core-halo (16%), irregular or multiply peaked (17%), spherical or unresolved (43%). Following above studies and Mac Low et al.(1991) the morphologies of the observed regions are described as following: Cometary regions have sharp leading edges with an approximately parabolic shape; Shells appear as a ring of emission at optically thin wavelengths; Core-halo objects have a central compact peak surrounded by a low surface brightness halo; Irregular objects have several peaks surrounded by a low surface brightness halo as well; Spherical objects have brightness distribution with Gaussian profiles which are sometimes unresolved (19%).

UCHIIs were modeled as bow-shock regions by Van Buren & MacCray (1988), Van Buren et al.(1990), Mac Low et al.(1991) and Van Buren & Mac Low (1992). Those models were necessary to get HII regions confined by ram pressure as the star moves along a cloud core, which could reproduce the small sizes ( $> 0.05$  pc) of UCHIIs. García-Segura & Franco (1996) (paper I, here after) showed that the ram pressure is not the only mechanism that can play an important rule. Instead, the thermal pressure within a cloud core can confine an UCHII in small sizes by its own. However, many of the UCHIIs show clearly a cometary shape, which in principle, would invoke stellar motions.

In this paper we have performed a number of models including stellar motions in order to account with all the ingredients that can play important rules, i.e., the ram pressure and the thermal one. Previous studies were based on thin-shell solutions for the computation of bow-shocks. Now, we present

<sup>1</sup>Instituto de Astronomía-UNAM-Ensenada, México.

<sup>2</sup>Instituto de Astronomía-UNAM-México.

gas dynamical simulations as a complement of paper I. The inclusion of stellar motion also give rise to very different situations as the stars leave their parental cloud cores and evolve into extended HII regions. All type of shapes can be expected for extended HII regions, which confirm previous predictions for the saw-tooth shapes of ionization fronts (paper I). The other novel aspect in this paper is that HII regions are calculated off-center from their parental clouds. Previous studies (Franco et al. 1990 and references therein) considered the stars located at the peak of the density structures, and so, those solutions are not appropriate for the cases studied here.

§2 describes the initial considerations and assumptions made in our paper. §3 explains and shows the gas dynamical simulations and §4 discusses the results and gives our conclusions.

## 2. INITIAL CONSIDERATIONS

For our study, we shall assume an isothermal cloud divided into an internal core of radius  $r_c$  and an external zone, for which  $P = \rho c_s^2$  ( $c_s = \text{constant}$ ) in hydrostatic equilibrium,

$$\vec{\nabla}P = -\rho \vec{g} \Rightarrow \vec{\nabla}\rho = -\frac{\rho}{c_s^2} \vec{g}. \quad (1)$$

Assuming that the cloud is spherically symmetric,  $\vec{\nabla} \rightarrow \frac{d}{dr}$ ;  $\vec{g} \rightarrow g_r$

$$\frac{d\rho}{dr} = -\frac{\rho}{c_s^2} g_r. \quad (2)$$

We first assume that the density structure in the external zone falls off as a power law  $r^{-2}$ , which is the case of a self-gravitating isothermal cloud:

$$\rho(r) = \rho_c (r/r_c)^{-2} \quad \text{for } r \geq r_c. \quad (3)$$

Solving for  $g_r$  using (2) and (3) we find

$$g_r = \frac{2 c_s^2}{r} = \frac{2 c_s^2}{r_c} (r/r_c)^{-1} \quad \text{for } r \geq r_c. \quad (4)$$

Inside the core,  $g_r$  must grow from zero up to  $2 c_s^2/r_c$ . Then, a simple manner is assuming that  $g_r$  grows linearly in this zone, such as  $g_r = A(r/r_c)$ . Thus, in order to join the external solution (4), we need that  $A = 2 c_s^2/r_c$ .

This imply that the density distribution inside the core is found integrating (2) with the new  $g_r$ , giving

$$\rho(r) = \rho_0 \exp\left[-(r/r_c)^2\right] \quad \text{for } r \leq r_c, \quad (5)$$

where  $\rho_0$  is the central density at  $r = 0$ . Making equal (3) and (5) at  $r = r_c \Rightarrow \rho_c = \rho_0/e$ .

In summary, the final solution for the density distribution of the cloud is given by

$$\rho(r) = \begin{cases} \rho_0 \exp\left[-(r/r_c)^2\right] & \text{for } r \leq r_c \\ \rho_0/e (r/r_c)^{-2} & \text{for } r \geq r_c \end{cases} \quad (6)$$

and the gravitational acceleration

$$g_r = \begin{cases} 2 c_s^2/r_c (r/r_c) & \text{for } r \leq r_c \\ 2 c_s^2/r_c (r/r_c)^{-1} & \text{for } r \geq r_c \end{cases} \quad (7)$$

We second assume, for the next set of simulations, that the density structure in the external zone falls off as a power law  $r^{-3}$ , and using the above approach, we find

$$\rho(r) = \begin{cases} \rho_0 \exp\left[-3/2 (r/r_c)^2\right] & \text{for } r \leq r_c \\ \exp(-3/2) \rho_0 (r/r_c)^{-3} & \text{for } r \geq r_c \end{cases} \quad (8)$$

and the gravitational acceleration

$$g_r = \begin{cases} 3 c_s^2/r_c (r/r_c) & \text{for } r \leq r_c \\ 3 c_s^2/r_c (r/r_c)^{-1} & \text{for } r \geq r_c \end{cases} \quad (9)$$

We third assume that the modeled stars were born in situ at their parental cloud, i.e., we are not modeling ‘run-away’ stars. The largest expected stellar velocity that such a cloud can produce is given by the dispersion velocity. Nothing that (see section 2.1 in paper I)  $P = 16/9 \pi G \rho_c^2 r_c^2 = \rho_c c^2$ , and solving for  $c$ , we find

$$c = 4.07 r_{0.1} n_6^{1/2} \text{ km s}^{-1} \quad (10)$$

where  $r_{0.1}$  is the core radius in units of 0.1 pc, and  $n_6$  the density in units of  $10^6 \text{ cm}^{-3}$ . Thus, stellar velocities up to  $\sim 13 \text{ km s}^{-1}$  can be considered in this study, for core densities of  $10^7 \text{ cm}^{-3}$  and for  $r_{0.1} = 1$ .

## 3. 2-D GAS DYNAMICAL SIMULATIONS

The numerical simulations are performed with the gas dynamical MHD code ZEUS-3D (version 3.4) (Stone & Norman 1992) (see paper I for details). We have chosen cartesian coordinates with the Y-axis being the symmetry axis (slab geometry) in this study. Thus, the star can be placed at any location along the X-Z plane. This particular choice is very safe, since it does not include any axis artifact in the computations (like in cylindrical coordinates).

The set up in all models is similar. The star is fixed on the computational mesh and it remains static during the computation. The stellar motion is then translated into a stream of gas in the whole

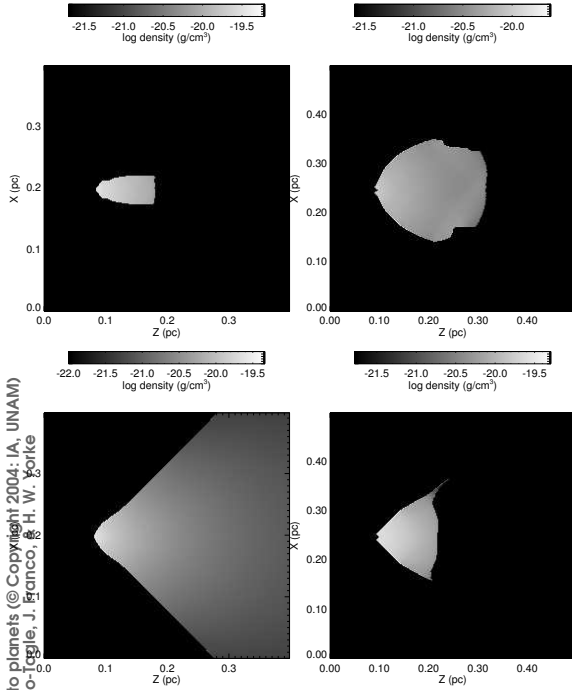


FIG. 1. Photoionized gas density snapshots for models A0 ( $t = 6 \times 10^5$  yr) ( $v_* = 0$  km s $^{-1}$ ) (top left), B0 ( $t = 6 \times 10^5$  yr) ( $v_* = 0$  km s $^{-1}$ ) (bottom left), A2 ( $t = 3.2 \times 10^5$  yr) ( $v_* = 2$  km s $^{-1}$ ) (top right) and B2 ( $t = 2 \times 10^5$  yr) ( $v_* = 2$  km s $^{-1}$ ) (bottom right).

computational mesh. During time, the outer boundary of the Z axis is updated with the oncoming gas at the stellar velocity. This update depends on the nature of the problem, i.e., it takes into account the slope of the ISM density distribution. All models have the same numerical resolution, being 250 zones along the X axis and 250 along Z.

We use the same approach of paper I to model the HII region (see Bodenheimer et al. 1979), i.e., we solve a radial integral to find the position of the Strömgen radius (Strömgen 1939), this time in cartesian coordinates. Then, the minimum temperature inside of the HII region is set to the photoionization equilibrium temperature ( $\sim 10^4$  K).

The modeling of a realistic UCHII which includes its stellar hypersonic wind (i.e., an ultracompact bubble) is very expensive in computational time, due to the fact that the winds from massive main sequence stars are of the order of  $10^3$  km s $^{-1}$ , when their bubble sizes are of the order of  $10^{-2}$  pc. This feature forces the Courant condition to calculate very small time-steps during the simulations. Thus, it is possible to include stellar winds in 2-D simulations that cover physical times of the order of  $10^3$  yr, but

very time consuming for 2-D simulations in which the physical times are of the order of  $10^5$  yr. For that reason, we have not include the effects of the stellar wind in the models. However, we showed in paper I that the size of the computed UCHII is mainly due to the thermal pressure of the ionized gas at these high densities. Thus, models A and B are qualitatively correct, without lost of generality.

To begin with our study, we first computed several cases (not shown in the paper) where the star is located at the center of the core given by (6). For a core radius of 0.1 pc, a central density of  $10^7$  cm $^{-3}$  and  $F_* = 10^{48}$  s $^{-1}$ , the models behaved very similar to the 1-D solutions computed in paper I. This is understandable, since the gaussian core of (6) produces a plateau at the center, which resembles the constant medium used in the first part of paper I. Thus, pressure equilibrium were achieved for all models at timescales which matched the one calculated in paper I. The novel aspect is that, since gravity is present in this study, the final density structure is affected by it. This important feature will be discussed below.

The second set of models without stellar motion (models A0 and B0) are calculated with the stars at the border of the core (Figure 1, left). The purpose of these models is to study the expansion and dynamic of the HII regions in the density ramps given by (6) and (8) for  $r \geq r_c$  respectively. Models labeled by A correspond to equation (6), while models B to equation (8). The number correspond to the stellar velocity. In both models, the ionized gas acquire a flat density distribution during the first forty thousand years in both cases, however, as time pass by, the ionized gas notices the cloud gravity and makes the necessary re-adjustments to become in hydrostatic equilibrium. This feature is clearly observable in model A0, where pressure equilibrium is achieved and the final density distribution follows the initial density ramp. Note however that the density decreases by a factor of  $\approx 200$ , since the hydrostatic equilibrium is achieve at  $10^4$  K, while initially was at  $10^2$  K. Model B0 on the other hand does not reach pressure equilibrium in the computational domain, and a blister-like region or champagne flow (Tenorio-Tagle 1979) is produced. Gas is permanently photoevaporated from the cloud, and this rise in a steady state mass loss rate from the cloud. Due to photoevaporation, the ionized gas does not follow the imposed ramp ( $\rho \propto r^{-3}$ ), and instead, the final solution is closer to the ramp of the type  $r^{-2}$ .

Note that the density ramps in these cases are off-centered from the stellar locations, i.e., the ori-

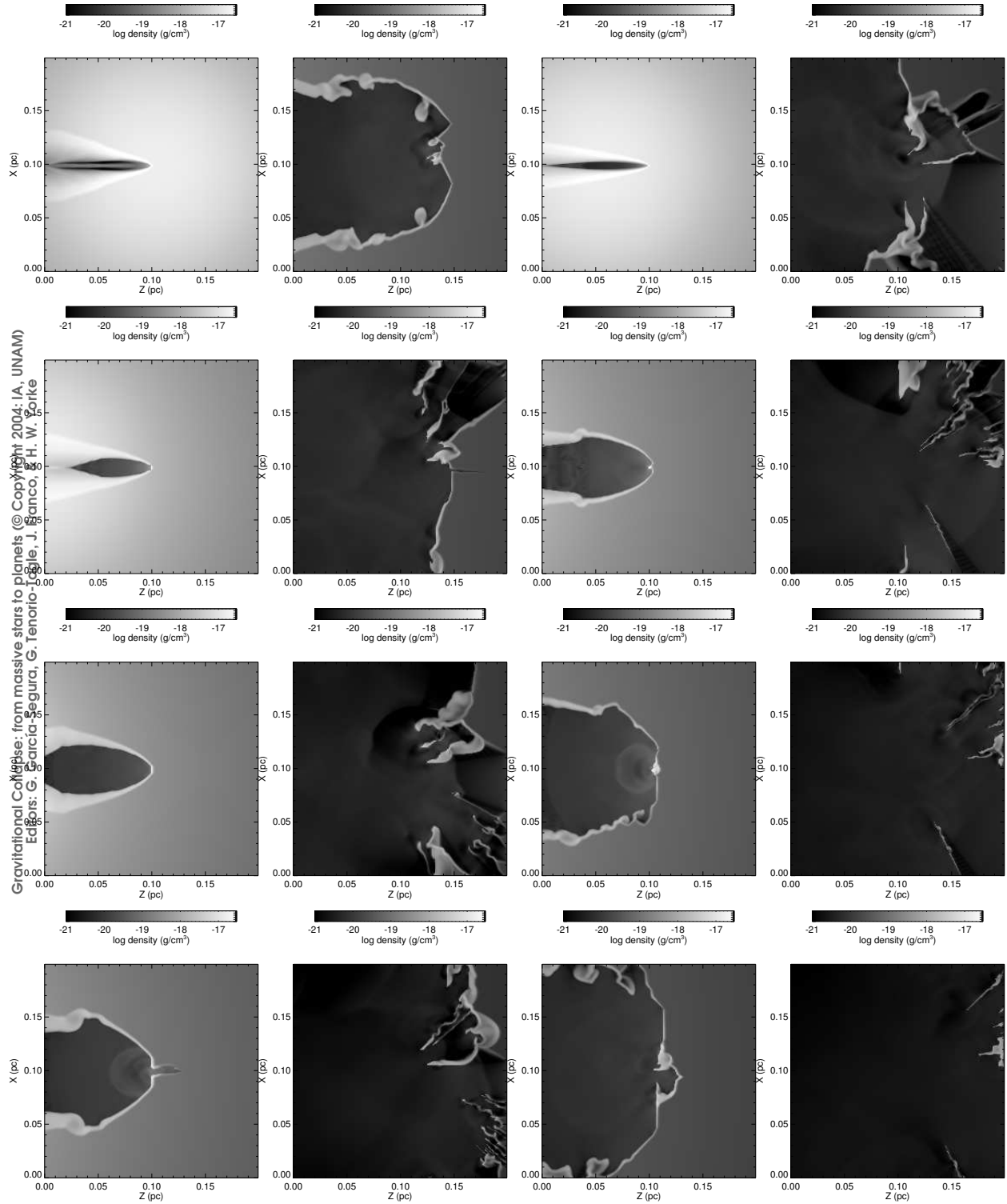


Fig. 2. Gas density, snapshots of two examples (B8 and B12) ( $v_* = 8, 12 \text{ km s}^{-1}$ ). Times in units of  $10^5$  years are (top to bottom): 0.12, 0.28, 0.4, 0.52, 0.64, 0.76, 0.88, 1 (for both models). The star departs at  $z = -0.1$  pc from the cloud center. The last stellar position correspond to 0.82 pc and 1.22 pc respectively from the cloud center.

gin of the power laws do not coincide with the stellar coordinates, and the solutions given by Franco et al. (1990) (and references therein) are not applicable. The third set of models (Figure 1 right, Figure 2) include stellar motion. The stars depart from the cloud center, and after crossing the gaussian cores, they encounter the density ramp described above. During the early stages inside the core, these models have a cometary shape due to a leading bow-shock, with sizes of the order of hypercompact HII regions. Once that they enter into the density ramp, their sizes grow in time, since the density is falling down, and depending of their velocities, they keep their cometary shapes for a period of time (high velocity cases, Figure 2) or turn quickly into blister type regions (low velocity cases, Figure 1 right). This is just because the expansion velocity of the HII regions can be smaller or larger than their stellar velocities respectively.

For example, Figure 1 shows that the shape of the ionized gas of models A0, B0, A2 and B2, which could be misclassified as cometary regions, are indeed blister type regions. Observationally, it must be difficult to classify these regions, unless proper motions were known.

Figure 2 is an example of how rich the variety of shapes could be, since the small scale structure found in the computations are always transients. The life time of these structures (elephant trunks) is proportional to the size of the HII region and inversely proportional to the stellar motion. The 7th frame in Figure 2 does not intend to explain the M16 pillars, since they are bigger by a factor of 50, but gives a guide about how the formation could be.

UCHIIs classified as core-halo can be explained by self-blocking effects when the stars comes into their leading piled-up clumps. A clear example of that is shown in frame 11 of figure 2.

To summarize, these type of models tell that, hypercompact and ultracompact HII regions are long

lived astronomical objects while they are inside of their parental cloud cores. When stars escape (as models A2 and B2) from those cores, transitions to larger structures as classical HII regions are expected. On the other hand, stars can fall back into the core by the gravitation potential of the cloud, forming smaller structures again.

Thus, the life-time of an ultracompact or a hypercompact HII region is just defined by the crossing time of the cloud core, simply given by

$$\tau_{ucHII} = r_c/v_*. \quad (11)$$

In cases where the stellar orbits are always smaller than the core radius, the life-time will be just the stellar life-time.

We thank Michael L. Norman and the Laboratory for Computational Astrophysics for the use of ZEUS-3D. This work is inspired by Bodenheimer et al. 1979.

## REFERENCES

- Bodenheimer, P., Tenorio-Tagle, G., & Yorke, H. W. 1979, *ApJ*, 233, 85  
 Franco, J., Tenorio-Tagle, G., & Bodenheimer, P. 1990, *ApJ*, 349, 126  
 García-Segura, G., & Franco, J. 1996, *ApJ*, 469, 171, paper I  
 Kurtz, S., Churchwell, E., & Wood, D. O. S. 1994, *ApJS*, 91, 659  
 Mac Low, M.-M., Van Buren, D., Wood, D. O. S., & Churchwell, E. 1991, *ApJ*, 369, 395  
 Stone, J. M., & Norman, M. L. 1992, *ApJS*, 80, 753  
 Strömgren, B. 1939, *ApJ*, 89, 526  
 Tenorio-Tagle, G. 1979, *A&A*, 71, 59  
 Van Buren, D., & Mac Low, M.-M. 1992, *ApJ*, 394, 534  
 Van Buren, D., Mac Low, M.-M., Wood, D.O.S., & Churchwell, E. 1990, *ApJ*, 353, 570  
 Van Buren, D., & McCray, R. 1988, *ApJ*, 329, L93  
 Wood, D. O. S., & Churchwell, E. 1989, *ApJS*, 69, 831